Therapeutic ultrasound transducer technology and monitoring techniques: a review with clinical examples

Maxime Lafond, Allison Payne, Cyril Lafon

Therapeutic ultrasound transducer technology and monitoring techniques: a review with clinical examples

Maxime Lafond[1], Allison Payne[2], and Cyril Lafon[1]

[1]LabTAU, INSERM, Centre Léon Bérard, Université Claude Bernard Lyon 1, F-69003, LYON, France
[2]Department of Radiology and Imaging Sciences, University of Utah, Salt Lake City, Utah, USA

Abstract

The exponential growth of therapeutic ultrasound applications demonstrates the power of the technology to leverage the combinations of transducer technology and treatment monitoring techniques to effectively control the preferred bioeffect to elicit the desired clinical effect. This review provides an overview of the most commonly used bioeffects in therapeutic ultrasound and describes existing transducer technologies and monitoring techniques to ensure treatment safety and efficacy. Effective combinations of these options are illustrated through descriptions of several clinical indications that have been successful in leveraging therapeutic ultrasound to provide effective patient treatments.

Keywords

Focused ultrasound, high intensity focused ultrasound, ultrasound transducer, ultrasound monitoring, therapeutic ultrasound

Introduction

In the surgeon's toolbox, most tools have a defined and specific use. In contrast, therapeutic ultrasound, utilizing the unique and simple phenomenon that is periodic succession of compression and expansion, can have a wide array of biological effects and is more comparable to a Swiss army knife than a scalpel. Ultimately, the tool you utilize is driven by

the desired clinical outcome. With that in mind, it should be highlighted that not all therapeutic ultrasound devices are created equal. Since the early days of the field followed by exponential growth that has occurred in the last few decades, therapeutic ultrasound technology and design has become more specialized and adapted to each particular application. This phenomenon can be broadly seen in transducer materials and designs, pulsing schemes, and monitoring techniques. This review will not cover the entirety of the field (an ambitious enterprise indeed), but aims to highlight key choices that are made in terms of transducer design, treatment parameters and procedure monitoring for specific clinical applications. The possibility of these combinations are highlighted in four applications, uterine fibroids, prostate disease, liver cancer and brain cancer, that are at different points along the path of clinical evaluation.

Bioeffects and acoustic exposure conditions

Therapeutic ultrasound applications have many benefits that have influenced the continuing development and adoption of this exciting technology for the treatment of a myriad of health conditions. This non-invasive, non-toxic and non-irradiating technology is highly flexible in that several different bioeffects can be elicited from the ultrasonic energy. Ultrasound induced biological effects are dependent on tissue properties, applied acoustic parameters and the presence of exogenous agents in the system, such as microbubbles or nanoparticles. Broadly speaking, bioeffects can be generally discretized into two categories: ablative and non-ablative mechanisms. Ablative biological effects typically result in cellular necrosis, tissue coagulation and generation of tissue debris [1]. Non-ablative effects can elicit increased blood flow [2] and tissue oxygenation [3], induce temporary stress and enhance tumor permeability. Both ablative and non-ablative effects can be achieved through both thermal and mechanical mechanisms. For the purposes of this review, thermal ablation and histotripsy will be

described as ablative techniques, while hyperthermia and mechanical stimulus will be described as non-ablative. Each category will be described with emphasis on the general acoustic parameters required to achieve the effect with consideration of the ultrasound transducer technology required to deliver and assess the biological effect.

Ablative effects:

Thermal ablation can be achieved by heating tissue to cytotoxic levels. While tumor cells can be more sensitive to temperature than normal cells due to variations in tissue hypoxia and pH [4,5], cell responses to heat elevation are dependent on both magnitude and duration of the thermal exposure. Thermal ablative therapies typically target temperature in the range of 55-80°C to denature structural and enzymatic proteins [6,7] and achieve tissue necrosis. Thermal dose is often used to assess the cumulative effects of thermal ablation. While several thermal dose models have been proposed for assessing thermal damage, the cumulative equivalent minutes 43°C (CEM43) model [8] is one of the most widely cited and often used as a benchmark metric for thermal treatments in both preclinical literature and clinical practice [9]. In therapeutic ultrasound, thermally ablative effects are generally achieved with a lower peak pressure but higher spatial-averaged time-averaged intensity (I_{SATA}) values that utilized in non-thermal approaches [10], usually above 1500 W/cm² [11]. To achieve thermal effects longer duty cycles are utilized (10-100%) with peak positive pressures in the 1-30 MPa range.

Non-thermal ablation can be achieved using histotripsy, a technique that uses short, high amplitude ultrasound pulses to leverage inertial cavitation or boiling. Both techniques produce similar lesions through tissue disintegration. When therapeutic ultrasound is applied, the rarefaction phase can transform endogenous cavitation nuclei into larger, ultrasound scattering bubbles on which the high-amplitude positive pressure scatters with phase inversion, propagating the cloud [12]. Upon sufficient rarefaction pressure, the transient

bubbles collapse and fragment, and the resulting mechanical strain can result in tissue damage [13]. The acoustic exposure to achieve histotripsy requires microsecond-long ultrasound bursts with a duty cycle of $\leq$ 1% minimizing tissue heating while generating cavitation effects through endogenous gas in tissues. Very high ultrasound intensities are required, typically > 30 kW/cm^2 I_{SPPA}, with high peak negative pressures (a range of pressures have been reported for varied applications [14,15]). Ultrasound transducers with relatively low operating frequency (1 MHz) [16], large apertures with low f-number [17] and a high focal gain [18] are needed to achieve these parameters [19]. Boiling histotripsy can be achieved with lower negative pressure (10-15MPa) but a much higher peak positive pressure, oftentimes forming a shock front, millisecond-long pulse durations and low pulse repetition frequency (PRF) of 0.5 to 1 Hz [20]. High frequencies are preferred (up to 3 MHz) to favor absorption and heating so each pulse generates boiling. A f-number (focal length divided by transducer aperture) of $>$1 is also typically utilized, as acoustic saturation occurs before shocks of sufficient amplitude can be formed to achieve boiling withing milliseconds.

Non-ablative effects:

If tissue is heated to non-ablative hyperthermic levels (<43°C), blood flow and oxygenation are increased as well as vascular permeability [2,21], but cell death can still be induced through apoptosis. Hyperthermia has been applied to both superficial and deep-seated tissues with a variety of single- [22] and multi-element [23] ultrasound transducers with frequencies of approximately 1 to 1.7 MHz, and for SATA intensities that were estimated at 0.7 to 8.8 kW/cm^2, respectively, based on the reported powers and focal dimensions [22,23]. Note that this estimation would place this in the ablative realm and is likely an over-estimate. Non-ablative mechanical stimulus is used in conjunction with micron-size gas bubbles to induce stable cavitation, resulting in the steady oscillation of the micro gas bubbles as a function of

pressure. This can result in tissue changes including membrane or blood vessel permeabilization and has been leveraged for extensive work in blood brain barrier opening, resulting in numerous preclinical studies from rodents to primates [24,25]. It should be noted that while the ultrasound induced biological effects have been presented as independently applied, multiple bioeffects are oftentimes triggered simultaneously. For example, mechanical perturbation can induce mild hyperthermia [26]. Similarly, acoustic exposures intended to induce heating can also be accompanied by non-thermal effects [27].

Transducer technology

Producing an ultrasound field for a specific therapeutic application requires two ingredients: the raw material producing the wave and the shape that allows it to reach the target. Nevertheless, several groups spiked the recipe along the years, innovating in transducer designs and use to allow higher efficacy, wider bandwidth, steering capabilities, etc. This section summarizes how the transducer technology produces ultrasound waves for therapeutic applications and how various design improvements proposed to optimize the produced pressure field.

Making waves

Therapeutic ultrasonic sources are usually made of piezoelectric ceramic. These materials deform under the action of an electric field, vibrate and generate ultrasound when applying voltages oscillating in the MHz range. These piezoelectric ceramic (often PZT, lead zirconium titanate) transducers have a narrow bandwidth and a high Q-factor with a wavelength λ that corresponds to twice the ceramic thickness. Piezocomposite transducers are manufactured by dicing piezoceramic crystals into pillars and filling the cuts with resin. This design results in larger bandwidths and more flexibility in terms of beam shaping. Even if the resin tends to limit the efficiency of these materials, they were also proposed for therapeutic

applications [28]. Their acoustic impedance, lower than that of ceramics, promotes the transfer of energy to coupling water and biological tissues. The piezocomposite materials are more suitable for arrays, such as those on the Ablatherm and Focal One devices [29], as the structure of the material limits transverse waves, crosstalk between elements and the electrical impedance of small elements but may be less robust than PZT for operating at high voltages because of intense internal stress between the resin and the piezo ceramic rods [30].

Different solutions for backing of the transducer have been proposed [28]. They all tend to use materials with very different acoustic impedance from the transducer to maximize the transfer of energy through the front face. A thin layer of air is often placed behind the transducer but solid solutions have also been used. The solid backing solutions make it possible to reinforce the mechanical structure of the transducer but also to cool the transducer from the rear in the case of continuous use.

Micromachined ultrasonic transducers (MUT) are micromachined electromechanical systems (MEMS). Capacitive MUT (CMUT) consist of a membrane suspended above a silicon substrate (wafer), with a cavity (or a defined thickness gap) in between. Both the cavity and the membrane are covered with a dielectric material, allowing tension and vibration of the membrane [31]. Piezoelectric MUT (PMUT) utilize the flexion mode of a piezoelectric membrane above a cavity in a silicon wafer [32]. MUTs provide many benefits such as broad bandwidth, ease of miniaturization and integration with electronics, making them ideal solutions for imaging [33,34]. This technology can be tuned in order to compete with conventional PZT in terms of pressure output [35]. For example, N'Djin et al. [36] integrated CMUTs into prototypes of interstitial devices and successfully induced thermal lesions in tissues under MR guidance [37]. However, the technical complexity of fabricating MUT in a standard laboratory compared to that of piezo-electric transducers limits its widespread adoption. Although one can expect these roadblocks to be eliminated as the

design and manufacturing improves, specifically as electrical and thermal robustness are the main constraints on CMUTs integrity [36].

Shaping the wave

Whatever the technology chosen for the transducer, it is possible to generate the high pressures necessary for the therapeutic effect by designing focused sources. Focusing is classically obtained by using a spherical source, but can also be obtained by positioning a spherical acoustic lens of appropriate shape and impedance on the front face of a flat transducer [38]. More complex focusing and steering capabilities and correcting for aberrations errors can be achieved with silicone acoustic lenses, cast in tailored 3-D printed molds [39–41]. It should be noted that silicone lenses attenuate the ultrasound wave, and from a practical point of view, can hinder cooling of the active surface. Focusing can also be achieved through building a network of elements and controlling individual element phases to electronically generate and steer a focus. This strategy has been made realistic by efficient and low-cost multi-channel driving electronics [42]. It is also possible to combine the two strategies of spherical sources and array transducers to maximize the pressure gain while allowing electronic deflection of the beam. Insightec's ExAblate Neuro device is a good illustration of this strategy [43]. A large hemisphere of 15 cm radius is cut into 1024 elements in order to deposit sufficient energy to produce a thalamotomy through the skull, to electronically move the focus to optimize the treatment and to adjust the surface power according to intervening tissues. This strategy is possible if the elements constituting the network are sufficiently small and therefore omnidirectional.

Periodic positioning of the elements results in grating lobes which can prove undesirable in the case of a therapeutic application as grating lobes can cause off-target treatment effects. In order to achieve good electronic focusing capabilities and to significantly

reduce grating lobes, Pernot et al. [44] proposed a quasi-random distribution of circular elements. Rosnitskiy et al. [45] proposed an array with Fermat's spiral distribution of Voronoi tessellation-shaped elements in order to increase the filling factor (and thus the focal gain in pressure) while maintaining electronic focusing capabilities. Shaping the transducer or using arrays of elements can also be used to meet a particular medical need. For instance, Melodelima et al. [46] proposed a toroidal transducer with 256 elements in order to produce a large conical focal zone and accelerate tissue ablation during surgical procedure. Flat, unfocused emitters are also an option for interstitial, transurethral and vascular applications, as well as in BBB opening as described in the last section of this review.

The conventional mode of vibration of a PZT transducer is along its thickness. However, this is not the only option. With the goal to build therapeutic ultrasound arrays with high element density similar to that of diagnostic ultrasound probes, with reduced electrical impedance, Hynynen and Yin [47] proposed driving the lateral mode of piezoceramic elements. Accordingly, Jones et al. [48] described a 256-element device where each element was composed of three concentric cylindrical lead zirconate titanate (PZT-4) allowing sonication at different frequencies. A 4096-element (PZT), densely populated transducer with $\lambda/2$ element spacing presented by Aslani et al. [49] is an interesting design that operates the elements in lateral mode to decouple the electrical impedance from frequency to eliminate the need for matching circuits. Its lower driving frequency (550 kHz) in conjunction with the small element spacing drastically reduces grating lobes. Lateral modes can also be harnessed to achieve a wider directivity in the context of intravascular US, such as in the Ekosonic endovascular system. This system notably allows treatment of peripheral arterial disease [50], deep vein thrombosis [51], and pulmonary embolism [52], and is being investigated for cavitation-mediated drug delivery to stabilize atheromas [53,54]. Pellow et al. [55] combined axial and lateral orthogonal electrical fields in order to control the directivity of a beam from

single piezoceramic elements and applied this strategy successfully to open the blood brain barrier in mice. In terms of efficiency, the pressure generated at the surface of a source can be increased by piling up transducers [56,57].

Most applications that use ultrasound for both therapy and imaging guidance combine two separate transducers dedicated for each purpose. They can be side by side, inserted into each other or back-to-back [58]. Depending on the exposure conditions needed to produce the desired bioeffect, different studies have proposed so-called dual-mode ultrasound arrays (DMUA), using the same transducer for both therapy and imaging. This approach obviously simplifies the registration between the imaging and therapeutic coordinate systems and may be advantageous to the application, even if compromises on the individual transducer performances must be made. In that context, Ebbini et al. presented a 64-element, 1 MHz prototype DMUA with imaging and therapeutic capabilities for thermal ablation [59]. In the continuation of this work, the same group performed successful preclinical tests with a dual mode probe of 64 elements for the thermal ablation of neurovascular structures for the treatment of hypertension [60]. Bouchoux et al. [61] designed a catheter with a rotating transducer for both imaging and thermal ablation. In order to favor emission for seconds-long durations, reduce the internal catheter heating and the duration of the impulse response, they combined a low-loss air-backed piezocomposite material operating at a frequency of 11 MHz, with front matching layers and a relevant electrical matching circuit. The transducer efficiency could be maintained at 71% and an impulse response corresponding to an axial resolution of 0.2 mm could be achieved. A transducer of similar design was used in the device described by Owen et al. and was evaluated in vivo [62], where thermal ablation under M-mode monitoring was achieved in liver with a 5-element mechanically oscillating dual mode applicator. Up to 27 W/cm^2 surface intensity was generated for seconds and impulse response length was 295 ± 1.0 ns at −6 dB. Daunizeau et al. went further in the miniaturization of the

catheter and the integration of the elements for improved beam steering capabilities [63]. Their 64-element probe generated a surface intensity of 20 W/cm^2, had an impulse response of 250 ns at -6 dB and offered a large axial focus steering (6-20 mm). DMUA were also proposed for treating with cavitation. Williams et al. [64] proposed such an array operating at 1 MHz. It was able to generate shock fronts of up to 45 MPa and peak negative pressures up to 9 MPa at focusing distances of 38–75 mm from the array. These performances were achieved while offering decent imaging capabilities, resolving centimeter-sized features in tissue at depths of 3–7 cm. 2D matrix arrays have been designed for blood brain barrier opening preclinical applications. Zhang et al. designed a piezoceramic array of 256 elements with a front matching layer operating at 1 MHz [65]. The obtained spatial resolution (>1.7mm) allowed the user to outline the brain of the rats but was not able to differentiate the different cerebral structures. On the therapy side, 3D control of the focal points and ms-long repeated pulses were feasible for sharp control of the location of BBB opening.

Treatment guidance

Regardless of whether the therapeutic ultrasound system utilizes dual mode ultrasound arrays, most bioeffects require treatment guidance and monitoring. These needs are a function of the type of bioeffect desired and can be achieved through a variety of methods. There have been several excellent reviews covering both ultrasound [9,66] and MRI techniques [67–69]. This summary complements these efforts.

For thermal applications of therapeutic ultrasound, thermal dosimetry should provide spatial and temporal data that is adequate to monitor the thermal changes induced by the treatment. Ideally, this should be monitored throughout the treatment with pre-treatment acquisition to assess measurement noise, treatment monitoring for tissue changes, and post-treatment acquisition to monitor the cool-down phase. It is known that thermal bioeffects are

cumulative [8], and accurate dosimetry is critical in assessing the extent of cell death and apoptosis. One of the most straightforward metrics of thermal change is temperature.

Magnetic resonance thermometry is the reference method used in several commercial therapeutic ultrasound devices in quasi real-time. While many parameters that influence the magnetic resonance imaging signal have a temperature dependence [68,70], the most frequently utilized technique for MR thermometry in soft tissues is the proton resonant frequency shift [71]. This method has been used to obtain precise in vivo temperature change measurements, with precisions of ~1°C often reported [72–74], when sufficient signal to noise ratio is achieved. However, the presence of the therapeutic ultrasound transducer and acoustic coupling medium in the MRI environment often make it difficult to place radiofrequency receive coils near the region of interest, greatly reducing the image SNR that can be achieved during treatment. While novel radiofrequency receive coils have been utilized in MRI guided therapeutic ultrasound [75–77], increasing the available SNR for MR thermometry, the presence of the therapeutic ultrasound ground plane has been found to impact MR image quality [78,79]. Careful consideration of the transducer position [76,77] and ground plane configuration [78,80] can improve image SNR, and subsequently, MR thermometry precision.

Efforts have been made to use ultrasound to measure temperature. These methods are mainly based on variations of sound speed with temperature. Tracking change in speckle allows measuring the thermal strain due to change of the speed of the sound and thus temperature [81–84]. This method requires knowing the variation of sound speed with temperature for all heated tissues. Generally speaking, the speed of sound peaks around 50°C. Beyond this point, the precision of measurements around this value is low and there may be ambiguity on the temperature due to the bijective nature of the function. Depending on the intensity of the heating and in order not to be sensitive to movements, speckle tracking methods require rapid imaging rates which are not always available in the clinic. These

limitations may factor in the fact that, to date, ultrasound thermometry is not coupled with a commercial therapeutic ultrasound device.

In ablative applications, heating is not an end in itself but a means to coagulate the target tissues. Although temperature monitoring is important, notably to ensure safety, ultrasonic methods can be employed to monitor directly tissue alterations. In certain tissues such as liver tissue, the coagulated areas are visible on conventional B-mode images [85]. However, these observations vary from one tissue to another depending on the changes in the attenuation and backscattering coefficients with temperature. High intensity focused ultrasound (HIFU) treatments in the prostate regularly induce hyper-echoic zones which are not necessarily an indicator of the thermal lesions obtained [86,87], mainly due to the transient nature of the changes [88]. Decorrelated compounding of synthetic aperture ultrasound imaging was proposed to improve the lesion contrast-to-noise ratio [89] and alternatives based on the processing of the signal backscattered by the tissue have therefore been developed. On the model of temperature measurements, Souchon et al. [90] used speckle tracking and echo strain at low frame rate to visualize the extent of high-intensity ultrasound-induced thermal lesions during their formation in vitro. Isoechoic lesions were detected in experimental echo-strain images as apparent expansion areas. Zhou et al. [91] developed a similar strategy for guiding ex vivo RF ablation, demonstrating that instantaneous echo decorrelation images was a good predictor of coagulation.

Backscattered signal processing methods were also proposed for monitoring thermal treatments by HIFU. At the forefront of these methods is Nakagami ultrasonic imaging, which allows tissue characterization based on the concentration and distribution of the speckle. The method consists in matching a statistical law on the pixel intensity distribution in a region of interest. The parameters of this Nagakami law vary with HIFU-induced tissue destruction. There is abundant literature describing preclinical validations of the method [92–96] but it

does not appear to be used clinically. Many other methods for statistical analysis of changes in RF lines during HIFU treatment have been proposed. As an example, the entropy parameter gave a better contrast of thermal lesions compared to standard B-mode images during HIFU ex vivo experiments [97].

The acoustic attenuation also changes with the tissue alterations induced during ultrasonic treatments [98]. Ribault et al. performed HIFU, creating lesions in ex vivo liver and estimated attenuation locally using the centroid and the multinarrow band methods before and after HIFU [99]. The zone with increased attenuation post HIFU correlated well with the ablated zone. Zderic et al. conducted similar experiments in vivo but with attenuation measurements performed in transmission [100]. The attenuation coefficient was higher in HIFU-treated tissues but this increase in attenuation was due to change in the tissue structure and presence of bubbles due to cavitation or boiling. Rahimian and Tavakkoli performed dynamic measurements of attenuation during HIFU treatments varying the intensity and the exposure duration to differentiate the increase in attenuation resulting from bubble activity generated from structural tissue change [101].

Besides alteration of the tissue itself, coagulation results in destruction of blood vessels and hardening of the tissues, providing opportunities for treatment monitoring using perfusion and elasticity measurements. Perfusion can be studied by ultrasound using contrast agents, which are micrometric-sized gas bubbles with lipid shells injected in the blood circulation. The encapsulated gas significantly increases the echogenicity. This lipid capsule stabilizes the gas bubbles and reduces their solubility for circulation times of several minutes. The circulation of these agents in the capillaries makes it possible to highlight devascularized areas such as coagulation necrosis induced by HIFU [102]. Gadolinium can be injected similarly in MRI to characterize induced tissue coagulation [103].

Photoacoustics refers to the generation of mechanical waves in an object illuminated by a laser beam. Absorbent nanoparticles can be injected, but depending on the wavelength applied, it is also possible to excite hemoglobin and therefore image blood vessels. It was demonstrated in vitro that the photoacoustic signal followed the process of HIFU-induced coagulation [104]. Lai et al. [105] also combined laser light and ultrasound for detecting thermal lesions in vitro but with a different modality called acousto-optic imaging. In this method, ultrasound affects the refractive index and displaces light scatterers. The collection of the ultrasound modulated light results in an image with the contrast of light and the spatial resolution of ultrasound. It was demonstrated that the acousto-optic signal could be used to follow the formation of thermal lesions.

Coagulation necrosis also leads to hardening of soft tissues and elastography is now a well-established technique for characterizing tissue elasticity. Elastography is an imaging modality based on the generation and monitoring of shear waves whose speed is directly proportional to tissue elasticity (shear modulus). This measurement can be done by different imaging modalities (e.g. MRI) but ultrasound allows it to be carried out in real time using ultra-fast scanners (speeds of several thousand frames per second). Lizzi et al. demonstrated ex vivo the feasibility of using the radiation force with ms-long pulses generated by the HIFU beam [106]. The displacements in the focal zone were tracked with a colinear diagnostic transducer in order to detect some change in the stiffness during the heating process. Curiel et al. pursued this approach in vivo but with local harmonic motion (HM) [107]. The amplitude of the vibration varied with its frequency and was a good indicator of the onset of thermal lesions. Han et al. used an imaging probe to follow HM and successfully performed real time lesion mapping in vivo [108]. Arnal et al. provided quantitative maps of tissue stiffness with a 4-fold increase in the presence of a thermal lesion ex vivo [109]. Shear wave elastography successfully detected RF- and HIFU-induced thermal lesions in vivo in real time [110,111].

More recently, Barrère et al used passive elastography to detect HIFU lesions in liver ex vivo [112]. This method does not require generating shear waves and relies on those naturally propagating in the body.

As seen in in the field of ultrasound imaging, artificial intelligence is showing promising perspectives in the monitoring HIFU lesions. Various tissue characteristics such as attenuation or backscattering coefficient, scaling parameter of Nakagami distribution, frequency-dependent scatterer amplitudes and tissue vibration can be estimated from RF data, combined and used as predictor of thermal lesions. Rangraz et al. performed ex vivo experiments, measured these parameters before and after HIFU and used them as features to train a neural network [113]. Lesions could be detected with a precision of 0.5 mm. Jia et al. extended this strategy to clinical data and tested different post-treatment image segmentation methods to optimize the detection of thermal lesions in the liver by HIFU [114].

A growing number of emerging applications rely on (or accidentally trigger) the phenomenon of ultrasound cavitation which should then be properly monitored to ensure both efficacy and safety. Particularly, undesired cavitation during thermal treatments in the brain are a concern [115,116]. While hyperechogenicity remains a mainstay of bubble detection in cavitation-based therapies [19], the oscillating bubbles under the action of an ultrasonic field also generate a very distinct noise which can be detected passively. Passive cavitation detectors (PCD) have been used for decades to detect and monitor cavitation activity [117–119]. Recent developments target the overall quantification of the cavitation dose using PCD [120,121]. As for spatial monitoring, a reduced number of hydrophones makes it possible to geolocate cavitation activity through correlation methods [122,123]. Imaging techniques using conventional imaging arrays such as passive acoustic mapping (PAM) of passive cavitation imaging (PCI) have been developed [124–127], but they all suffer from weak spatial resolution in the axial direction, perpendicular to the array (typically of the order of 1

cm) because of the relatively small aperture. This is even more critical for applications requiring a 3D monitoring of the cavitation activity. Indeed, even if a few works have demonstrated the feasibility of 3D passive acoustic mapping of cavitation [128,129], the poor quality of images due to very low apertures of conventional matrix arrays, or the complexity of the devices specifically designed, limits the pertinence of 3D passive imaging techniques. However, it is possible to control or regulate the level of cavitation in order to ensure a therapeutic response [130]. Multiple strategies for better visualization of the cavitation extent are under investigation. Adaptive beamforming such as the robust Capon method have shown great results in improving the axial resolution, with the drawback of a heavy computational cost [131]. Like the current trend in PCD, quantification is also of great interest in imaging [132–136]. However, linking the signal location with actual bioeffect is not straightforward, notably due to the complex relation between the cavitation cloud behavior and the scattered and emitted acoustic signals. A first step is the classic dichotomy between stable and inertial cavitation, which can be imaged selectively by beamforming on specific frequency bands [136]. While these two phenomena are occurring on a spectrum and most likely colocalized, their relative proportions can be visualized using compositing [135].

There are numerous techniques that can be utilized for therapeutic ultrasound treatment monitoring. Because ultrasound is applied non-invasively, the monitoring technique must be carefully considered to adequately assess the bioeffect to ensure not only treatment efficacy, but patient safety as well.

Clinical Indications

As in ultrasound imaging, the treatment of specific organs requires the development of specialized devices meeting anatomical constraints. In order to illustrate the therapeutic and technological options reviewed in earlier sections, the authors have decided to describe two

established clinical applications and two emerging clinical applications of therapeutic ultrasound: ultrasound-induced thermal ablation of prostate cancer, image-guided treatment of uterine fibroids by HIFU, cavitation for opening the blood-brain barrier in treating brain cancers, and histotripsy for the mechanical ablation of liver cancers.

Image-guided treatment of uterine fibroids by HIFU

Two extracorpeal focused ultrasound systems have been developed to thermally ablate uterine fibroids under MRI guidance: the Insightec ExAblate [137] and the Sonalleve (developed by Philips Healthcare and transferred to Profound Medical in 2017) [138]. Both systems utilize a spherically curved, phased array transducer designed to allow for deep tissue penetration and beam steering around the geometric focus. The ExAblate system has a phased array transducer with 208 elements arranged in a hybrid sector-vortex and concentric ring pattern. The transducer operates within a 0.96-1.14 MHz frequency range and has a 12 cm aperture [34]. Importantly, the system allows mechanical movement of the transducer in multiple directions to achieve the desired clinical thermal effect and allows avoidance of near and far-field structures that could impede the beam path or cause undesired tissue damage [10]. The Sonalleve system is similar in that the transducer is a spherically curved phased array (256 elements in a random sparse pattern, 12 cm radius of curvature, 13 cm aperture) operated at a center frequency of 1.2 MHz. This system creates volumetric thermal ablation through electronically steering through concentric trajectories via a controller that uses MR thermometry as feedback [138]. In both systems, treatment monitoring and assessment are achieved through MR-derived thermal [139] and vascular biomarkers [140]. The treatments are largely effective and importantly allow the patients a much shorter recovery time when compared to more mainstream procedures such as uterine artery embolization and surgical hysterectomy. The flat, large aperture transducer design by Aslani et al. [49] has been

evaluated in a first-in-human in a uterine fibroid study, demonstrating the novel design overcomes some of the limiting factors of the smaller aperture fibroid ultrasound transducers, particularly in the limitations of electronic steering and near field heating due to element spacing. Their results demonstrated that there was no off-target heating in any of the eleven treated patients. While the lower operating frequency of this transducer (550 kHz compared to ~1 MHz of other systems) resulted in less near-field heating, allowing for more rapid ablation rates, far-field heating particularly around boney structures was a concern.

Uterine fibroid treatments were also accomplished using ultrasound guidance. The JC200D1 device (Haifu Medical Technology Co. Chongqing, China) uses single-element ultrasound transducer (0.8 MHz frequency, radius of curvature 15 cm, aperture 20 cm) and utilizes a point scanning method to cover the desired treatment volume, where the treatment is monitored through a combination of blood flow or gray scale changes in the ultrasound images [141]. Similar to MRI, contrast enhanced imaging can be utilized as a vascular biomarker to determine the non-perfused volume of the treated fibroid area [142]. Other treatments have been achieved with the JC200, ExAblate MRgFUS, and Sonalleve systems including palliative treatment of bone metastases [143–145], unresectable pancreatic tumors [146] and desmoid tumors [147].

Ultrasound-induced thermal ablation of prostate tissue

Focused ultrasound technologies have also been used extensively for the thermal ablation treatment of prostate cancer since the 1990s with treatment of diseased prostate tissues approved by the FDA in 2015. An extracorporeal approach proved difficult due to the deep position of the prostate in the pelvis. As it is located just behind the rectum, the first treatments proposed an endorectal approach with sources operating at relatively high frequencies. The Sonablate (Focus Surgery, Indianapolis, IN, USA) is an ultrasound-guided

single element 4 MHz transrectal probe [148] that utilizes both low and high intensity modes (1300-2200 W/cm2) to achieve thermal ablation [149]. The Ablatherm (EDAP-Technomed, Lyon, France) is also a transrectal device that uses a single element 3 MHz transducer for treatment with a separate imaging array (7.5 MHz) used for treatment monitoring. Automated probe displacements allow precise treatment of the entire prostate [150]. The treatment was carried out under ultrasound guidance to define the position of the prostate and the volume to be treated. The coagulated volume does not appear clearly on conventional ultrasound. Alternatively, it can be estimated either by backscattered energy measurements [151] or by the use of contrast ultrasound [152]. Thanks to the possibility of measuring temperature by MRI, new devices have been proposed using endo-rectal [153] or endo-urethral [154] approaches. The Exablate 2100 Prostate system (Haifa, Israel) utilizes a transrectal, approximately 1000 element phased array transducer that operates at 2.3 MHz. The TULSA-PRO system is a transurethral system that utilizes a 10-element (5 x 4 mm, 4 or 13 MHz frequency, acoustic power 0 to 4 W) transducer that allows the user to select which elements are used for treatment [155].

Large-scale clinical trials demonstrated that HIFU-induced whole gland ablation is a potentially effective treatment of localized prostate cancer, with a low cancer-specific mortality rate and a high metastasis-free survival rate at 10 years as well as acceptable morbidity [156]. Exposure conditions can be adjusted to take into account the properties of the tissues and treat patients who have benefited from radiotherapy [157]. Progress in the field of prostate cancer diagnosis through the use of multi-modality MRI [158] has made it possible to better define the extent of the cancer and to develop more precise and less invasive focal treatment. A large clinical study with the Sonablate system on carefully selected 1379 patients with clinically significant prostate cancer demonstrated a good cancer control with HIFU-induced focal therapy over 7 years regardless of risk [159]. Electronic steering of the focus

was integrated in the Focal One device (EDAP-Technomed) as an evolution of the Ablatherm. This device is composed of 16 co-centric annular elements that allows the user to alter the focus of the transducer between 32 and 67 mm from the transducer face. This provides the option to create longer lesions by altering the phasing of the transducer elements. A recent prospective trial demonstrated that in 91 patients, focal treatment using this device resulted in good functional outcomes with half of the patients remaining cancer-free after 3 years [160]. To the author's knowledge, there are currently no publications that describe comparative clinical trials between therapeutic ultrasound and other modalities of ablation of prostate cancer. There are only retrospective studies with paired patients comparing HIFU with laparoscopic [161] or robotic radical prostatectomy [162,163]. These studies all demonstrated that HIFU treatment was a valid option for all the prostate cancer types considered.

Histotripsy for the mechanical ablation of liver cancers

Clinical studies demonstrating the ability of histotripsy to destroy tissue are present in the literature. The Theresa study [164] was a phase I study that evaluated the use of the VORTX system (Histosonics, Ann Arbor, MI) [19] to treat end-stage liver tumors. The VORTX system is equipped with a therapeutic transducer (700 kHz) has an in-line imaging probe (7.5 MHz) to non-invasively delivers low duty cycle (<1%), high peak negative pressure (>10 MPa) acoustic exposures to create a bubble cloud that induces mechanical cellular destruction. In all treated patients in this trial (N=8), an ablation was created per the treatment plan, and demonstrated the safety of the device. The subsequent #HOPE4LIVER trials NCT04572633 and NCT04573881 [165] enrolled 47 and 24 patients, respectively. While the final results of these studies were not published at the time of writing of the presented review, the 95.5% technical success and limited complication rates (6.8%) led to the clearance of the Edison System by the FDA.

Blood brain barrier opening for treating brain cancer

The use of ultrasound to open the BBB in combination with microbubbles has been widely studied. Reports indicated the technique as safe in animals since 2001 [166]. Ultrasound-induced BBB opening has now reached clinical evaluation. In this section, we briefly describe the systems with published clinical work on BBB opening in brain cancer.

The ExAblate series system is a widely used transcranial, MR-guided, FUS solution developed and manufactured by InSightec (Haifa, Israel). The ExAblate Model 4000 ("ExAblate Neuro") obtained the CE marking for functional neurosurgery in 2012. It consists or a "helmet-like" stereotactic frame and comprises 1024 transducers. The "low-frequency" version of the system operates around 220 kHz for BBB opening, while the "mid-frequency" version operates around 650 kHz for thermal ablation [167]. The cavitation needed for BBB opening is permitted by injection of Definity microbubbles, injected immediately before each treatment location, [168]. Cavitation occurrence is ensured by incrementally increasing the power until subharmonic detection, at which point power is halved, typically around the 500 kPa mark [169].The practical ExAblate Neuro clinical workflow, notably the treatment monitoring, was been described by Meng et al. [170]. For BBB opening, the treatment planning is performed by drawing a polygon around a treatment volume on the MRI. It should be noted that the ultrasound power is not changed during all the points within the targeted volume but the level of cavitation activity is acquired. Tissue heating is not expected in BBB opening procedure due to the low pressure (~500 kPa) and duty cycle (effective 0.74% at each treatment spot) [169]. However, MR can be used in to evaluate microhemorrhages using T2*-weighted gradient echo and susceptibility-weighted sequences. T1-weighted MRI after gadolinium injection can assess the extent of BBB opening at the end of the treatment. The ExAblate Neuro system was used in a phase I, single-arm, open-label study, in which five

patients with high grade glioma tumors underwent FUS in combination with chemotherapy one day prior to surgical resection [168]. T1-weighted MRI revealed a 15-50% increase in contrast enhancement. The BBB opening was transient (under 20 hours). The same group performed a single-arm, open-label trial with 9 glioblastoma patients (NCT03616860) [171]. Successful BBB opening was confirmed by increased areas of gadobutrol (604 Da) enhancement, and decrease in the enhancement the next day, demonstrating BBB permeability restoration.

Unlike the stereotactic Exablate system, NaviFUS (Taiwan) is a frameless device, operating with a neuronavigation system. The NaviFUS systems consists of 256 elements operating at 500 kHz. It is devised to induce BBB opening when combining the US field with Sonovue microbubbles (MBs). During treatment sequences, at each location, the output is ramped up until detection of acoustic emissions using 16 of the elements defined as receivers, then ramped down to a given in situ mechanical index (MI, rarefaction pressure in MPa divided by the square root of the frequency in MHz) value (typically in the 0.5-0.68 range) and maintained for 120 seconds. The (PRF is 9 Hz and the burst duration 10 ms (duty cycle 0.9%). Treatment planning is based on regions of interest defined from T1 enhanced and/or T2 high signal regions. CT scans are also performed to obtain bone porosity information. Then, FUS simulations are performed to estimate transcranial pressure distribution and transmission and calculating an optimal probe positions and order to treat the defined ROIs. Successful opening of the BBB can be assessed by dynamic contrast-enhanced MRI. In clinical trial NCT03626896, Chen et al. evaluated BBB opening detection with the dynamic contrast-enhanced MRI. MIs of 0.48, 0.58, and 0.68 were used [172]. K_{trans} and V_e were calculated and demonstrated increased BBB permeability after treatment. A pilot study combining MB-FUS-mediated BBB opening with radiotherapy (NCT01628406) reported results from 6 patients with recurrent malignant high-grade glioma [173]. The range of MI

was 0.53-0.61, based on the previous clinical data [174]. No control of successful BBB opening was performed in this specific study. Transient BBB opening by MB-FUS was also evaluated in recurrent glioblastoma patients in a prospective, open-label, single-center, single-arm phase 1 clinical trial involved 6 patients (NCT04446416) [172] for efficacy and safety assessment of the device in combination with bevacizumab. Results of the trial were not published at the time of writing of this review paper.

The SonoCloud devices series, developed by Carthera (France), differs from the NaviFUS and ExAblate systems as it is an implantable solution. For treatment of glioblastoma, the SonoCloud device is implanted within the skull bone, overlying the tumor area, following tumor resection. The BBB opening is subsequently done in an ambulatory fashion under local anesthesia. Neuronavigation systems can be used to position the device at the desired location. The SonoCloud-1 implants consists of a single, unfocused, 10-mm diameter transducer operating at 1.05 MHz. It is encased in a 11.5-mm diameter housing. The transducer is driven using a transdermal needle connected to the implant and powered by a designated external signal generator. The pulsing scheme used in the reported clinical settings is 25,000-cycle bursts at 0.5 or 1 Hz PRF (1.2 or 2.4% duty cycle), applied for 150 to 270 seconds. The peak pressure produced by the SonoCloud-1 varies between 0.41 and 1.15 MPa (measured in water), which is sensibly higher than what is used in the ExAblate and NaviFUS systems. The authors reported that the optimal pressure range was 0.90-1.03 MPa. There is no monitoring or assessment of cavitation activity during treatment, but BBB opening, subsequently quantified on MRI correlates with the local acoustic pressure [175].

The SonoCloud-1 was first evaluated in a single-arm, single-center trial (NCT02253212) [176,177]. A total of 21 patients were included and 19 received at least one sonication. Following BBB opening procedure, patients were split in two groups depending on the extent of BBB opening assessed on MR images. Clear BBB disruption was associated

with higher median progression-free and overall survival compared to no or poor BBB opening (in months: 4.11 vs 2.73 PFS and 12.94 vs 9.64 OS). While this is a promising finding, Sonabend and Stupp highlighted a few limitations as a commentary [178]. Namely, the insufficient number of patients to show efficacy, and the small volume of BBB opening. The latter issue is mostly corrected as the SonoCloud device was also presented as a network of 3 and 9 transducers (SonoCloud-3 and SonoCloud-9), covering a much larger treatment volume. In 6-patient cohort, the SonoCloud-3 device was shown to be as well-tolerated as the SonoCloud-1. The SonoCloud-9 was also investigated in combination with carboplatin in an open-label, single arm, multicenter phase 1/2a clinical trial involving 38 participants (NCT03744026). Dose escalation was performed by increasing the number of active transducers. Another trial (NCT04528680) investigated the SonoCloud-9 in combination with albumin-bound paclitaxel or carboplatin. The authors reported carboplatin and paclitaxel concentration increases of 5.9 and 3.7 times, respectively [179]. A challenge, admitted by the authors, was the variability across patients, attributed to tumor heterogeneity on susceptibility to treatment. One can hypothesize that variability in tumor acoustic properties can also induce variability in the extent of BBB opening and that a certain degree of treatment monitoring could improve the outcome. In their recent developments, the SonoCloud-9 was tested on 33 patients with recurrent glioblastoma, in combination with carboplatin [180]. While interpretation of their results is limited due to the small cohorts, findings support the hypothesis of improved efficacy with higher concentrations of drugs in the brain at the time of sonications.

Discussion

The field of therapeutic ultrasound covers a vast variety of bioeffects, parameter range, and monitoring modalities. The choice of each of these items is ideally dictated by the targeted

organ and the bioeffect sought, but is oftentimes dictated by the technology used in laboratories in the early phases. However, despite technological constraints, there are multiple ways to achieve a desirable bioeffect in a target tissue. We hope to demonstrate this in an attempt at better visualizing our complex field. We share an interactive representation based on the papers cited in this review article. We hope the reader will take some time to explore how the field – at least the narrow representative window presented here – is interconnected. To do so, we labeled each article of this review (when applicable) with the criteria presented in Table 1. The table was imported into the visualization online platform KUMU, accessible with this link: https://kumu.io/MaximeLafond/lafond-payne-lafon-ijhreview#references-visualization (Please contact one of the authors in case of issue accessing the visualization). The visualization provides actionable filters and clustering features. Examples of representations, namely bioeffects and pressure range clustering (Figure 1), and bioeffects and monitoring techniques (Figure 2), are presented as examples.

This review focused on highlighted four applications, uterine fibroid, prostate disease, liver cancer and brain cancer, that are currently at different points in the clinical evaluation path. For each of them, there are several ongoing (recruiting) clinical trials, as outlined briefly in Table 2, with a more detailed examination in Supplementary Table 1. Based on the ever-expanding research being conducted in preclinical realms, it is apparent that additional clinical applications of therapeutic ultrasound, utilizing a myriad of bioeffects will continue to grow and improve in the coming years. It is important to keep in mind that while new and innovative monitoring techniques, transducer designs and ever-expanding applications are exciting and provide great opportunities for developments, the continued investigation of all bioeffects, particularly in large clinical trials that demonstrate efficacy should not be dismissed or overlooked. Disrupting improvements can be made even at this stage by change

in the treatment strategy, for example focal treatment instead of whole gland in prostate cancer ablation, or changes in bioeffects (mechanical or thermal ablation).

Moving forward from technical developments to clinical evaluation, it should be noted that information on acoustic conditions (acoustic intensity, peak pressure, pulsing scheme) becomes gradually sparser. As clinical translation progresses, it is likely that physicians weigh in decisions regarding guidance and monitoring choices. This calls for integrative metrics of ultrasound exposure or built-in bioeffect assessment methods to ensure reproducibility of studies amongst clinical systems, cohorts, and clinical centers. The appropriate reporting guidelines of both acoustic exposure [181] and treatment parameters [182] have been well addressed in the literature. This accurate reporting is particularly critical when attempting to correlate a biological effect to acoustic exposure.

Therapeutic ultrasound will continue to improve in the next decades as the combination of transducer technology and treatment monitoring techniques will continue to evolve and be translated in clinical settings, leading to more personalized and efficient therapeutic ultrasound mediated therapies.

Acknowledgements: Funding was provided by the National Institute of Health under grant R37CA224141 and R01CA259686.

Declaration of Interest Statement: Dr. Lafon is a co-founder and industrial grant recipient from Carthera. Dr. Lafon and Dr. Lafond have received industrial grants from EDAP TMS.

Author Contribution: All authors contributed equally to the conception, researching, and writing of this work.

Data Availability Statement: Because this is a review article, there is not a data set associated with the paper as all information and data is derived from other works. Note the aggregation of literature data that is presented can be found at https://kumu.io/MaximeLafond/lafond-payne-lafon-ijhreview#references-visualization.

References

[1] Joiner JB, Pylayeva-Gupta Y, Dayton PA. Focused ultrasound for immunomodulation of the tumor microenvironment. J Immunol. 2020;205:2327–2341.
[2] Song CW, Rhee JG, Levitt SH. Blood flow in normal tissues and tumors during hyperthermia. J Natl Cancer Inst. 1980;64:119–124.
[3] Song CW, Park H, Griffin RJ. Improvement of tumor oxygenation by mild hyperthermia. Radiat Res. 2001;155:515–528.
[4] Knavel EM, Brace CL. Tumor ablation: common modalities and general practices. Tech Vasc Interv Radiol. 2013;16:192–200.
[5] Overgaard J. Influence of extracellular pH on the viability and morphology of tumor cells exposed to hyperthermia. J Natl Cancer Inst. 1976;56:1243–1250.
[6] Lepock JR. Cellular effects of hyperthermia: relevance to the minimum dose for thermal damage. Int J Hyperthermia. 2003;19:252–266.
[7] Eyerly SA, Vejdani- Jahromi M, Dumont DM, et al. The Evolution of Tissue Stiffness at Radiofrequency Ablation Sites During Lesion Formation and in the Peri- Ablation Period. J Cardiovasc Electrophysiol. 2015;26:1009–1018.
[8] Sapareto SA, Dewey WC. Thermal dose determination in cancer therapy. Int J Radiat Oncol Biol Phys. 1984;10:787–800.
[9] Rivens I, Shaw A, Civale J, et al. Treatment monitoring and thermometry for therapeutic focused ultrasound. Int J Hyperth Off J Eur Soc Hyperthermic Oncol North Am Hyperth Group. 2007;23:121–139.
[10] Payne A, Chopra R, Ellens N, et al. AAPM Task Group 241: A medical physicist's guide to MRI- guided focused ultrasound body systems. Med Phys [Internet]. 2021 [cited 2024 Mar 5];48. Available from: https://aapm.onlinelibrary.wiley.com/doi/10.1002/mp.15076.
[11] ter Haar G. Therapeutic applications of ultrasound. Prog Biophys Mol Biol. 2007;93:111–129.
[12] Maxwell AD, Wang T-Y, Cain CA, et al. Cavitation clouds created by shock scattering from bubbles during histotripsy. J Acoust Soc Am. 2011;130:1888.
[13] Mancia L, Vlaisavljevich E, Xu Z, et al. Predicting Tissue Susceptibility to Mechanical Cavitation Damage in Therapeutic Ultrasound. Ultrasound Med Biol. 2017;43:1421–1440.
[14] Maxwell AD, Owens G, Gurm HS, et al. Noninvasive Treatment of Deep Venous Thrombosis Using Pulsed Ultrasound Cavitation Therapy (Histotripsy) in a Porcine Model. J Vasc Interv Radiol. 2011;22:369–377.
[15] Xu J, Bigelow TA, Nagaraju R. Precision control of lesions by high-intensity focused ultrasound cavitation-based histotripsy through varying pulse duration. IEEE Trans Ultrason Ferroelectr Freq Control. 2013;60:1401–1411.

[16] Vlaisavljevich E, Lin K-W, Warnez MT, et al. Effects of tissue stiffness, ultrasound frequency, and pressure on histotripsy-induced cavitation bubble behavior. Phys Med Biol. 2015;60:2271.
[17] Vlaisavljevich E, Gerhardson T, Hall TL, et al. Effects of f-number on the histotripsy intrinsic threshold and cavitation bubble cloud behavior. Phys Med Biol. 2017;62:1269–1290.
[18] Maxwell AD, Yuldashev PV, Kreider W, et al. A prototype therapy system for transcutaneous application of boiling histotripsy. IEEE Trans Ultrason Ferroelectr Freq Control. 2017;64:1542–1557.
[19] Xu Z, Hall TL, Vlaisavljevich E, et al. Histotripsy: the first noninvasive, non-ionizing, non-thermal ablation technique based on ultrasound. Int J Hyperthermia. 2021;38:561–575.
[20] Canney MS, Khokhlova VA, Bessonova OV, et al. Shock-Induced Heating and Millisecond Boiling in Gels and Tissue Due to High Intensity Focused Ultrasound. Ultrasound Med Biol. 2010;36:250–267.
[21] Song CW, Park HJ, Lee CK, et al. Implications of increased tumor blood flow and oxygenation caused by mild temperature hyperthermia in tumor treatment. Int J Hyperthermia. 2005;21:761–767.
[22] Gray MD, Lyon PC, Mannaris C, et al. Focused Ultrasound Hyperthermia for Targeted Drug Release from Thermosensitive Liposomes: Results from a Phase I Trial. Radiology. 2019;291:232–238.
[23] Guthkelch AN, Carter LP, Cassady JR, et al. Treatment of malignant brain tumors with focused ultrasound hyperthermia and radiation: results of a phase I trial. J Neurooncol. 1991;10:271–284.
[24] Meng Y, Hynynen K, Lipsman N. Applications of focused ultrasound in the brain: from thermoablation to drug delivery. Nat Rev Neurol. 2021;17:7–22.
[25] Vykhodtseva NI, Hynynen K, Damianou C. Histologic effects of high intensity pulsed ultrasound exposure with subharmonic emission in rabbit brain in vivo. Ultrasound Med Biol. 1995;21:969–979.
[26] De Bever JT, Odéen H, Hofstetter LW, et al. Simultaneous MR thermometry and acoustic radiation force imaging using interleaved acquisition. Magn Reson Med. 2018;79:1515–1524.
[27] Baker KG, Robertson VJ, Duck FA. A Review of Therapeutic Ultrasound: Biophysical Effects. Phys Ther. 2001;81:1351–1358.
[28] Chapelon J-Y, Cathignol D, Cain C, et al. New piezoelectric transducers for therapeutic ultrasound. Ultrasound Med Biol. 2000;26:153–159.
[29] Curiel L, Chavrier F, Souchon R, et al. 1.5-D high intensity focused ultrasound array for non-invasive prostate cancer surgery. IEEE Trans Ultrason Ferroelectr Freq Control. 2002;49:231–242.
[30] Closset E, Trompette P, Birer A, et al. Numerical field intensity factor calculations for 1-3 piezocomposite structures. IEEE Trans Ultrason Ferroelectr Freq Control. 2006;53:2140–2151.
[31] Haller MI, Khuri-Yakub BT. A surface micromachined electrostatic ultrasonic air transducer. IEEE Trans Ultrason Ferroelectr Freq Control. 1996;43:1–6.
[32] Bernstein JJ, Finberg SL, Houston K, et al. Micromachined high frequency ferroelectric sonar transducers. IEEE Trans Ultrason Ferroelectr Freq Control. 1997;44:960–969.
[33] Brenner K, Ergun AS, Firouzi K, et al. Advances in capacitive micromachined ultrasonic transducers. Micromachines. 2019;10:152.
[34] Herickhoff CD, van Schaijk R. cMUT technology developments. Z Für Med Phys. 2023;33:256–266.

[35] Lee BC, Nikoozadeh A, Park KK, et al. High-efficiency output pressure performance using capacitive micromachined ultrasonic transducers with substrate-embedded springs. Sensors. 2018;18:2520.
[36] N'Djin WA, Gerold B, Vion-Bailly J, et al. Capacitive micromachined ultrasound transducers for interstitial high-intensity ultrasound therapies. IEEE Trans Ultrason Ferroelectr Freq Control. 2017;64:1245–1260.
[37] Suarez-Castellanos IM, de Sallmard G, Vanstaevel G, et al. Dynamic Ultrasound Focusing and Centimeter-Scale Ex Vivo Tissue Ablations With a CMUT Probe Developed for Endocavitary HIFU Therapies. IEEE Trans Ultrason Ferroelectr Freq Control. 2023;70:1470–1481.
[38] Woodacre JK, Landry TG, Brown JA. Fabrication and characterization of a 5 mm\times 5 mm aluminum lens-based histotripsy transducer. IEEE Trans Ultrason Ferroelectr Freq Control. 2022;69:1442–1451.
[39] Maimbourg G, Houdouin A, Deffieux T, et al. 3D-printed adaptive acoustic lens as a disruptive technology for transcranial ultrasound therapy using single-element transducers. Phys Med Biol. 2018;63:025026.
[40] Maimbourg G, Houdouin A, Deffieux T, et al. Steering capabilities of an acoustic lens for transcranial therapy: numerical and experimental studies. IEEE Trans Biomed Eng. 2019;67:27–37.
[41] Jiménez N, Romero-García V, Picó R, et al. Nonlinear focusing of ultrasonic waves by an axisymmetric diffraction grating embedded in water. Appl Phys Lett. 2015;107:204103.
[42] Hall T, Cain C. A Low Cost Compact 512 Channel Therapeutic Ultrasound System For Transcutaneous Ultrasound Surgery. AIP Conf Proc. 2006;829:445–449.
[43] Elias WJ, Lipsman N, Ondo WG, et al. A Randomized Trial of Focused Ultrasound Thalamotomy for Essential Tremor. N Engl J Med. 2016;375:730–739.
[44] Pernot M, Aubry J-F, Tanter M, et al. High power transcranial beam steering for ultrasonic brain therapy. Phys Med Biol. 2003;48:2577.
[45] Rosnitskiy PB, Vysokanov BA, Gavrilov LR, et al. Method for designing multielement fully populated random phased arrays for ultrasound surgery applications. IEEE Trans Ultrason Ferroelectr Freq Control. 2018;65:630–637.
[46] Melodelima D, N'Djin WA, Parmentier H, et al. Thermal ablation by high-intensity-focused ultrasound using a toroid transducer increases the coagulated volume. Results of animal experiments. Ultrasound Med Biol. 2009;35:425–435.
[47] Hynynen K, Yin J. Lateral mode coupling to reduce the electrical impedance of small elements required for high power ultrasound therapy phased arrays. IEEE Trans Ultrason Ferroelectr Freq Control. 2009;56:557–564.
[48] Jones RM, Deng L, Leung K, et al. Three-dimensional transcranial microbubble imaging for guiding volumetric ultrasound-mediated blood-brain barrier opening. Theranostics. 2018;8:2909.
[49] Aslani P, Huang Y, Lucht BBC, et al. A Fully Electronically Steerable Therapeutic Ultrasound Phased Array With MR-Guidance. IEEE Trans Biomed Eng. 2024;71:574–582.
[50] Goldstein JA, Mishkel G. Choosing the correct therapeutic option for acute limb ischemia. Interv Cardiol. 2011;3:381–390.
[51] Dumantepe M, Tarhan IA, Ozler A. Treatment of chronic deep vein thrombosis using ultrasound accelerated catheter-directed thrombolysis. Eur J Vasc Endovasc Surg. 2013;46:366–371.
[52] Khan K, Yamamura D, Vargas C, et al. The Role of EkoSonic Endovascular System or EKOS® in Pulmonary Embolism. Cureus. 2019;11:e6380.
[53] Kennedy SR, Lafond M, Haworth KJ, et al. Initiating and imaging cavitation from infused echo contrast agents through the EkoSonic catheter. Sci Rep. 2023;13:6191.

[54] Klegerman ME, Moody MR, Huang S-L, et al. Demonstration of ultrasound-mediated therapeutic delivery of fibrin-targeted pioglitazone-loaded echogenic liposomes into the arterial bed for attenuation of peri-stent restenosis. J Drug Target. 2023;31:109–118.
[55] Pellow C, Li S, Delgado S, et al. Biaxial ultrasound driving technique for small animal blood–brain barrier opening. Phys Med Biol. 2023;68:195006.
[56] Sferruzza J-P, Birer A, Chavrier F, et al. Damping, amplitude, aging tests of stacked transducers for shock wave generation. IEEE Trans Ultrason Ferroelectr Freq Control. 2002;49:1453–1460.
[57] Sferruzza JP, Birer A, Cathignol D. Generation of very high pressure pulses at the surface of a sandwiched piezoelectric material. Ultrasonics. 2000;38:965–968.
[58] Lim HG, Kim H, Kim K, et al. Thermal ablation and high-resolution imaging using a back-to-back (BTB) dual-mode ultrasonic transducer: In vivo results. Sensors. 2021;21:1580.
[59] Ebbini ES, Yao H, Shrestha A. Dual-Mode Ultrasound Phased Arrays for Image-Guided Surgery. Ultrason Imaging. 2006;28:65–82.
[60] Aravalli RN, Helden DV, Liu D, et al. Precision Targeted Ablation of Fine Neurovascular Structures In Vivo Using Dual-mode Ultrasound Arrays. Sci Rep. 2020;10:9249.
[61] Bouchoux G, Lafon C, Berriet R, et al. Dual-mode ultrasound transducer for image-guided interstitial thermal therapy. Ultrasound Med Biol. 2008;34:607–616.
[62] Owen NR, Chapelon JY, Bouchoux G, et al. Dual-mode transducers for ultrasound imaging and thermal therapy. Ultrasonics. 2010;50:216–220.
[63] Daunizeau L, Nguyen A, Le Garrec M, et al. Robot-assisted ultrasound navigation platform for 3D HIFU treatment planning: Initial evaluation for conformal interstitial ablation. Comput Biol Med. 2020;124:103941.
[64] Williams RP, Karzova MM, Yuldashev PV, et al. Dual-Mode 1-D Linear Ultrasound Array for Image-Guided Drug Delivery Enhancement Without Ultrasound Contrast Agents. IEEE Trans Ultrason Ferroelectr Freq Control. 2023;70:693–707.
[65] Zhang Z, Liu R, Li G, et al. A dual-mode 2D matrix array for ultrasound image-guided noninvasive therapy. IEEE Trans Biomed Eng. 2021;68:3482–3490.
[66] Lewis MA, Staruch RM, Chopra R. Thermometry and ablation monitoring with ultrasound. Int J Hyperth Off J Eur Soc Hyperthermic Oncol North Am Hyperth Group. 2015;31:163–181.
[67] Odéen H, Parker DL. Magnetic resonance thermometry and its biological applications–Physical principles and practical considerations. Prog Nucl Magn Reson Spectrosc. 2019;110:34–61.
[68] Rieke V, Butts Pauly K. MR thermometry. J Magn Reson Imaging. 2008;27:376–390.
[69] Winter L, Oberacker E, Paul K, et al. Magnetic resonance thermometry: Methodology, pitfalls and practical solutions. Int J Hyperth Off J Eur Soc Hyperthermic Oncol North Am Hyperth Group. 2016;32:63–75.
[70] Parker DL, Smith V, Sheldon P, et al. Temperature distribution measurements in two- dimensional NMR imaging. Med Phys. 1983;10:321–325.
[71] Poorter JD. Noninvasive MRI thermometry with the proton resonance frequency method: Study of susceptibility effects. Magn Reson Med. 1995;34:359–367.
[72] Quesson B, Laurent C, Maclair G, et al. Real- time volumetric MRI thermometry of focused ultrasound ablation *in vivo* : a feasibility study in pig liver and kidney. NMR Biomed. 2011;24:145–153.
[73] Ramsay E, Mougenot C, Köhler M, et al. MR thermometry in the human prostate gland at 3.0T for transurethral ultrasound therapy. J Magn Reson Imaging. 2013;38:1564–1571.

[74] Rieke V, Instrella R, Rosenberg J, et al. Comparison of temperature processing methods for monitoring focused ultrasound ablation in the brain. J Magn Reson Imaging. 2013;38:1462–1471.
[75] Corea J, Ye P, Seo D, et al. Printed Receive Coils with High Acoustic Transparency for Magnetic Resonance Guided Focused Ultrasound. Sci Rep. 2018;8:3392.
[76] Wharton IP, Rivens IH, Ter Haar GR, et al. Design and development of a prototype endocavitary probe for high-intensity focused ultrasound delivery with integrated magnetic resonance imaging. J Magn Reson Imaging JMRI. 2007;25:548–556.
[77] Minalga E, Payne A, Merrill R, et al. An 11-Channel Radio Frequency Phased Array Coil for Magnetic Resonance Guided High Intensity Focused Ultrasound of the Breast. Magn Reson Med Off J Soc Magn Reson Med Soc Magn Reson Med. 2013;69:295–302.
[78] Payne A, Minalga E, Merrill R, et al. Technical Note: Effect of transducer position and ground plane configuration on image quality in MR- guided focused ultrasound therapies. Med Phys. 2020;47:2350–2355.
[79] Hadley JR, Odéen H, Merrill R, et al. Improving image quality in transcranial magnetic resonance guided focused ultrasound using a conductive screen. Magn Reson Imaging. 2021;83:41–49.
[80] Lechner-Greite SM, Hehn N, Werner B, et al. Minimizing eddy currents induced in the ground plane of a large phased-array ultrasound applicator for echo-planar imaging-based MR thermometry. J Ther Ultrasound. 2016;4:4.
[81] Civale J, Rivens I, Ter Haar G, et al. Calibration of ultrasound backscatter temperature imaging for high-intensity focused ultrasound treatment planning. Ultrasound Med Biol. 2013;39:1596–1612.
[82] Varghese T, Zagzebski JA, Chen Q, et al. Ultrasound monitoring of temperature change during radiofrequency ablation: preliminary in-vivo results. Ultrasound Med Biol. 2002;28:321–329.
[83] Maass-Moreno R, Damianou CA, Sanghvi NT. Noninvasive temperature estimation in tissue via ultrasound echo-shifts. Part II. In vitro study. J Acoust Soc Am. 1996;100:2522–2530.
[84] Simon C, VanBaren P, Ebbini ES. Two-dimensional temperature estimation using diagnostic ultrasound. IEEE Trans Ultrason Ferroelectr Freq Control. 1998;45:1088–1099.
[85] Lafon C, Koszek L, Chesnais S, et al. Feasibility of a transurethral ultrasound applicator for coagulation in prostate. Ultrasound Med Biol. 2004;30:113–122.
[86] Sanghvi NT, Foster RS, Bihrle R, et al. Noninvasive surgery of prostate tissue by high intensity focused ultrasound: an updated report. Eur J Ultrasound. 1999;9:19–29.
[87] Illing RO, Leslie TA, Kennedy JE, et al. Visually directed high-intensity focused ultrasound for organ-confined prostate cancer: A proposed standard for the conduct of therapy. BJU Int. 2006;98:1187–1192.
[88] Puijk RS, Ruarus AH, Scheffer HJ, et al. Percutaneous Liver Tumour Ablation: Image Guidance, Endpoint Assessment, and Quality Control. Can Assoc Radiol J. 2018;69:51–62.
[89] Nguyen M, Zhao N, Xu Y, et al. Decorrelated compounding of synthetic aperture ultrasound imaging to detect low contrast thermal lesions induced by focused ultrasound. Ultrasonics. 2023;134:107098.
[90] Souchon R, Bouchoux G, Maciejko E, et al. Monitoring the formation of thermal lesions with heat-induced echo-strain imaging: A feasibility study. Ultrasound Med Biol. 2005;31:251–259.
[91] Zhou Z, Wang Y, Song S, et al. Monitoring microwave ablation using ultrasound echo decorrelation imaging: an ex vivo study. Sensors. 2019;19:977.

[92] Zhang S, Shang S, Han Y, et al. Ex vivo and in vivo monitoring and characterization of thermal lesions by high-intensity focused ultrasound and microwave ablation using ultrasonic Nakagami imaging. IEEE Trans Med Imaging. 2018;37:1701–1710.
[93] Zhang S, Zhou F, Wan M, et al. Feasibility of using Nakagami distribution in evaluating the formation of ultrasound-induced thermal lesions. J Acoust Soc Am. 2012;131:4836–4844.
[94] Han M, Song W, Zhang F, et al. Modeling for Quantitative Analysis of Nakagami Imaging in Accurate Detection and Monitoring of Therapeutic Lesions by High-Intensity Focused Ultrasound. Ultrasound Med Biol. 2023;49:1575–1585.
[95] Rangraz P, Behnam H, Tavakkoli J. Nakagami imaging for detecting thermal lesions induced by high-intensity focused ultrasound in tissue. Proc Inst Mech Eng [H]. 2014;228:19–26.
[96] Huang S-M, Liu H-L, Li D-W, et al. Ultrasonic Nakagami Imaging of High-intensity Focused Ultrasound-induced Thermal Lesions in Porcine Livers: Ex Vivo Study. Ultrason Imaging. 2018;40:310–324.
[97] Monfared MM, Behnam H, Rangraz P, et al. High-intensity focused ultrasound thermal lesion detection using entropy imaging of ultrasound radio frequency signal time series. J Med Ultrasound. 2018;26:24.
[98] Techavipoo U, Varghese T, Chen Q, et al. Temperature dependence of ultrasonic propagation speed and attenuation in excised canine liver tissue measured using transmitted and reflected pulses. J Acoust Soc Am. 2004;115:2859–2865.
[99] Ribault M, Chapelon JY, Cathignol D, et al. Differential Attenuation Imaging for the Characterization of High Intensity Focused Ultrasound Lesions. Ultrason Imaging. 1998;20:160–177.
[100] Zderic V, Keshavarzi A, Andrew MA, et al. Attenuation of porcine tissues in vivo after high-intensity ultrasound treatment. Ultrasound Med Biol. 2004;30:61–66.
[101] Rahimian S, Tavakkoli J. Estimating dynamic changes of tissue attenuation coefficient during high-intensity focused ultrasound treatment. J Ther Ultrasound. 2013;1:14.
[102] Rouvière O, Gelet A, Crouzet S, et al. Prostate focused ultrasound focal therapy—imaging for the future. Nat Rev Clin Oncol. 2012;9:721–727.
[103] Hijnen NM, Elevelt A, Grüll H. Stability and Trapping of Magnetic Resonance Imaging Contrast Agents During High-Intensity Focused Ultrasound Ablation Therapy. Invest Radiol. 2013;48:517.
[104] Cui H, Yang X. Real-time monitoring of high-intensity focused ultrasound ablations with photoacoustic technique: An *in vitro* study: Real-time monitoring HIFU with PAI. Med Phys. 2011;38:5345–5350.
[105] Lai P, McLaughlan JR, Draudt AB, et al. Real-time monitoring of high-intensity focused ultrasound lesion formation using acousto-optic sensing. Ultrasound Med Biol. 2011;37:239–252.
[106] Lizzi FL, Muratore R, Deng CX, et al. Radiation-force technique to monitor lesions during ultrasonic therapy. Ultrasound Med Biol. 2003;29:1593–1605.
[107] Curiel L, Chopra R, Hynynen K. In vivo monitoring of focused ultrasound surgery using local harmonic motion. Ultrasound Med Biol. 2009;35:65–78.
[108] Han Y, Wang S, Payen T, et al. Fast lesion mapping during HIFU treatment using harmonic motion imaging guided focused ultrasound (HMIgFUS) in vitro and in vivo. Phys Med Biol. 2017;62:3111.
[109] Arnal B, Pernot M, Tanter M. Monitoring of thermal therapy based on shear modulus changes: II. Shear wave imaging of thermal lesions. IEEE Trans Ultrason Ferroelectr Freq Control. 2011;58:1603–1611.

[110] Mariani A, Kwiecinski W, Pernot M, et al. Real time shear waves elastography monitoring of thermal ablation: in vivo evaluation in pig livers. J Surg Res. 2014;188:37–43.
[111] Kwiecinski W, Bessière F, Colas EC, et al. Cardiac shear-wave elastography using a transesophageal transducer: application to the mapping of thermal lesions in ultrasound transesophageal cardiac ablation. Phys Med Biol. 2015;60:7829.
[112] Barrere V, Melodelima D, Catheline S, et al. Imaging of thermal effects during high-intensity ultrasound treatment in liver by passive elastography: a preliminary feasibility in vitro study. Ultrasound Med Biol. 2020;46:1968–1977.
[113] Rangraz P, Behnam H, Shakhssalim N, et al. A feed-forward neural network algorithm to detect thermal lesions induced by high intensity focused ultrasound in tissue. J Med Signals Sens. 2012;2:192.
[114] Jia X, Li X, Shen T, et al. Monitoring of thermal lesions in ultrasound using fully convolutional neural networks: A preclinical study. Ultrasonics. 2023;130:106929.
[115] Maimbourg G, Houdouin A, Santin M, et al. Inside/outside the brain binary cavitation localization based on the lowpass filter effect of the skull on the harmonic content: a proof of concept study. Phys Med Biol. 2018;63:135012.
[116] Lafon C, Moore D, Eames MD, et al. Evaluation of Pseudorandom sonications for reducing cavitation with a clinical neurosurgery HIFU device. IEEE Trans Ultrason Ferroelectr Freq Control. 2020;68:1224–1233.
[117] Cleveland RO, Sapozhnikov OA, Bailey MR, et al. A dual passive cavitation detector for localized detection of lithotripsy-induced cavitation in vitro. J Acoust Soc Am. 2000;107:1745–1758.
[118] Tung Y-S, Vlachos F, Choi JJ, et al. In vivo transcranial cavitation threshold detection during ultrasound-induced blood-brain barrier opening in mice. Phys Med Biol. 2010;55:6141–6155.
[119] Chettab K, Mestas J-L, Lafond M, et al. Doxorubicin Delivery into Tumor Cells by Stable Cavitation without Contrast Agents. Mol Pharm. 2017;14:441–447.
[120] Ambekar PA, Wang Y-N, Khokhlova T, et al. Comparative Study of Histotripsy Pulse Parameters Used to Inactivate Escherichia coli in Suspension. Ultrasound Med Biol. 2023;49:2451–2458.
[121] Rich KT, Holland CK, Rao MB, et al. Characterization of cavitation-radiated acoustic power using diffraction correction. J Acoust Soc Am. 2018;144:3563–3574.
[122] Lafond M, Asquier N, Mestas JA, et al. Evaluation of a Three-Hydrophone Method for 2-D Cavitation Localization. IEEE Trans Ultrason Ferroelectr Freq Control. 2018;65:1093–1101.
[123] Hu Z, Xu L, Chien C-Y, et al. Three-dimensional Transcranial Microbubble Cavitation Localization by Four Sensors. IEEE Trans Ultrason Ferroelectr Freq Control. 2021;1–1.
[124] Salgaonkar VA, Saurabh Datta, Datta S, et al. Passive cavitation imaging with ultrasound arrays. J Acoust Soc Am. 2009;126:3071–3083.
[125] Gyöngy M, Coussios C-C. Passive spatial mapping of inertial cavitation during HIFU exposure. IEEE Trans Biomed Eng. 2010;57:48–56.
[126] Coviello C, Kozick R, Choi J, et al. Passive acoustic mapping utilizing optimal beamforming in ultrasound therapy monitoring. J Acoust Soc Am. 2015;137:2573–2585.
[127] Boulos P, Varray F, Poizat A, et al. Weighting the passive acoustic mapping technique with the phase coherence factor for passive ultrasound imaging of ultrasound-induced cavitation. IEEE Trans Ultrason Ferroelectr Freq Control. 2018;65:2301–2310.
[128] Sivadon A, Varray F, Béra J-C, et al. 3-D Passive Cavitation Imaging Using Adaptive Beamforming and Matrix Array Transducer With Random Apodization. IEEE Trans Ultrason Ferroelectr Freq Control. 2024;71:238–254.

[129] O'Reilly MA, Jones RM, Kullervo Hynynen, et al. Three-Dimensional Transcranial Ultrasound Imaging of Microbubble Clouds Using a Sparse Hemispherical Array. IEEE Trans Biomed Eng. 2014;61:1285–1294.
[130] Mondou P, Mériaux S, Nageotte F, et al. State of the art on microbubble cavitation monitoring and feedback control for blood-brain-barrier opening using focused ultrasound. Phys Med Biol. 2023;68.
[131] Coviello CM, Faragher SR, Coussios C-C. Robust Capon beamforming for passive cavitation mapping during high-intensity focused ultrasound therapy. J Acoust Soc Am. 2010;128:2280–2280.
[132] Yang Y, Zhang X, Ye D, et al. Cavitation dose painting for focused ultrasound-induced blood-brain barrier disruption. Sci Rep. 2019;9:1–10.
[133] Imran KM, Tintera B, Morrison HA, et al. Improved Therapeutic Delivery Targeting Clinically Relevant Orthotopic Human Pancreatic Tumors Engrafted in Immunocompromised Pigs Using Ultrasound-Induced Cavitation: A Pilot Study. Pharmaceutics. 2023;15:1585.
[134] Escudero DS, Haworth KJ, Genstler C, et al. Quantifying the Effect of Acoustic Parameters on Temporal and Spatial Cavitation Activity: Gauging Cavitation Dose. Ultrasound Med Biol. 2023;
[135] Lafond M, Salido NG, Haworth KJ, et al. Cavitation Emissions Nucleated by Definity Infused through an EkoSonic Catheter in a Flow Phantom. Ultrasound Med Biol. 2021;47:693–709.
[136] Haworth KJ, Bader KB, Rich KT, et al. Quantitative Frequency-Domain Passive Cavitation Imaging. IEEE Trans Ultrason Ferroelectr Freq Control. 2017;64:177–191.
[137] Tempany CMC, Stewart EA, McDannold N, et al. MR Imaging–guided Focused Ultrasound Surgery of Uterine Leiomyomas: A Feasibility Study. Radiology. 2003;226:897–905.
[138] Köhler MO, Mougenot C, Quesson B, et al. Volumetric HIFU ablation under 3D guidance of rapid MRI thermometry: Volumetric HIFU ablation with 3D rapid MRI thermometry. Med Phys. 2009;36:3521–3535.
[139] Yoon S-W, Cha SH, Ji YG, et al. Magnetic resonance imaging-guided focused ultrasound surgery for symptomatic uterine fibroids: estimation of treatment efficacy using thermal dose calculations. Eur J Obstet Gynecol Reprod Biol. 2013;169:304–308.
[140] McDannold N, Tempany CM, Fennessy FM, et al. Uterine Leiomyomas: MR Imaging–based Thermometry and Thermal Dosimetry during Focused Ultrasound Thermal Ablation. Radiology. 2006;240:263–272.
[141] Liu Y, Zhang WW, He M, et al. Adverse effect analysis of high-intensity focused ultrasound in the treatment of benign uterine diseases. Int J Hyperthermia. 2018;35:56–61.
[142] Peng S, Hu L, Chen W, et al. Intraprocedure contrast enhanced ultrasound: the value in assessing the effect of ultrasound-guided high intensity focused ultrasound ablation for uterine fibroids. Ultrasonics. 2015;58:123–128.
[143] Liberman B, Gianfelice D, Inbar Y, et al. Pain Palliation in Patients with Bone Metastases Using MR-Guided Focused Ultrasound Surgery: A Multicenter Study. Ann Surg Oncol. 2009;16:140–146.
[144] Hurwitz MD, Ghanouni P, Kanaev SV, et al. Magnetic resonance–guided focused ultrasound for patients with painful bone metastases: phase III trial results. J Natl Cancer Inst. 2014;106:dju082.
[145] Harding D, Giles SL, Brown MRD, et al. Evaluation of quality of life outcomes following palliative treatment of bone metastases with magnetic resonance-guided high intensity focused ultrasound: an international multicentre study. Clin Oncol. 2018;30:233–242.

[146] Vidal-Jove J, Perich E, Del Castillo MA. Ultrasound guided high intensity focused ultrasound for malignant tumors: the Spanish experience of survival advantage in stage III and IV pancreatic cancer. Ultrason Sonochem. 2015;27:703–706.
[147] Zhang R, Chen J-Y, Zhang L, et al. The safety and ablation efficacy of ultrasound-guided high-intensity focused ultrasound ablation for desmoid tumors. Int J Hyperthermia. 2021;38:89–95.
[148] Rewcastle JC. High Intensity Focused Ultrasound for Prostate Cancer: A Review of the Scientific Foundation, Technology and Clinical Outcomes. Technol Cancer Res Treat. 2006;5:619–625.
[149] Uchida T, Shoji S, Nakano M, et al. Transrectal high- intensity focused ultrasound for the treatment of localized prostate cancer: Eight- year experience. Int J Urol. 2009;16:881–886.
[150] Cordeiro ER, Cathelineau X, Thüroff S, et al. High- intensity focused ultrasound (HIFU) for definitive treatment of prostate cancer. BJU Int. 2012;110:1228–1242.
[151] Seip R, Sanghvi NT, Fedewa RJ, et al. 1H-2 Prediction of Success for HIFU Treatments of Prostate Cancer Based on Acoustic Energy Density. 2006 IEEE Ultrason Symp [Internet]. IEEE; 2006 [cited 2024 Mar 7]. p. 732–735. Available from: https://ieeexplore.ieee.org/abstract/document/4152052/.
[152] Rouvière O, Glas L, Girouin N, et al. Prostate Cancer Ablation with Transrectal High-Intensity Focused Ultrasound: Assessment of Tissue Destruction with Contrast-enhanced US. Radiology. 2011;259:583–591.
[153] Ehdaie B, Tempany CM, Holland F, et al. MRI-guided focused ultrasound focal therapy for patients with intermediate-risk prostate cancer: a phase 2b, multicentre study. Lancet Oncol. 2022;23:910–918.
[154] Burtnyk M, Hill T, Cadieux-Pitre H, et al. Magnetic Resonance Image Guided Transurethral Ultrasound Prostate Ablation: A Preclinical Safety and Feasibility Study with 28-Day Followup. J Urol. 2015;193:1669–1675.
[155] Anttinen M, Mäkelä P, Suomi V, et al. Feasibility of MRI-guided transurethral ultrasound for lesion-targeted ablation of prostate cancer. Scand J Urol. 2019;53:295–302.
[156] Crouzet S, Chapelon JY, Rouvière O, et al. Whole-gland ablation of localized prostate cancer with high-intensity focused ultrasound: oncologic outcomes and morbidity in 1002 patients. Eur Urol. 2014;65:907–914.
[157] Hostiou T, Gelet A, Chapelon J, et al. Salvage high- intensity focused ultrasound for locally recurrent prostate cancer after low- dose- rate brachytherapy: oncological and functional outcomes. BJU Int. 2019;124:746–757.
[158] Turkbey B, Huang R, Vourganti S, et al. Age-related changes in prostate zonal volumes as measured by high-resolution magnetic resonance imaging (MRI): a cross-sectional study in over 500 patients. BJU Int. 2012;110:1642–1647.
[159] Reddy D, Peters M, Shah TT, et al. Cancer control outcomes following focal therapy using high-intensity focused ultrasound in 1379 men with nonmetastatic prostate cancer: a multi-institute 15-year experience. Eur Urol. 2022;81:407–413.
[160] Kaufmann B, Raess E, Schmid FA, et al. Focal therapy with HIGH- INTENSITY focused ultrasound for prostate cancer: 3- year outcomes from a prospective trial. BJU Int. 2023;bju.16213.
[161] Nyk Ł, Michalak W, Szempliński S, et al. High-Intensity Focused-Ultrasound Focal Therapy Versus Laparoscopic Radical Prostatectomy: A Comparison of Oncological and Functional Outcomes in Low- and Intermediate-Risk Prostate Cancer Patients. J Pers Med. 2022;12:251.

[162] Albisinni S, Aoun F, Bellucci S, et al. Comparing High-Intensity Focal Ultrasound Hemiablation to Robotic Radical Prostatectomy in the Management of Unilateral Prostate Cancer: A Matched-Pair Analysis. J Endourol. 2017;31:14–19.
[163] Arnouil N, Gelet A, Matillon X, et al. [Focal HIFU vs robot-assisted total prostatectomy: Functionnal and oncologic outcomes at one year]. Progres En Urol J Assoc Francaise Urol Soc Francaise Urol. 2018;28:603–610.
[164] Vidal-Jove J, Serres X, Vlaisavljevich E, et al. First-in-man histotripsy of hepatic tumors: the THERESA trial, a feasibility study. Int J Hyperthermia. 2022;39:1115–1123.
[165] Wah TM, Pech M, Thormann M, et al. A Multi-centre, Single Arm, Non-randomized, Prospective European Trial to Evaluate the Safety and Efficacy of the HistoSonics System in the Treatment of Primary and Metastatic Liver Cancers (#HOPE4LIVER). Cardiovasc Intervent Radiol. 2023;46:259–267.
[166] Hynynen K, McDannold N, Vykhodtseva N, et al. Noninvasive MR Imaging–guided Focal Opening of the Blood-Brain Barrier in Rabbits 1. Radiology. 2001;220:640–646.
[167] Krishna V, Sammartino F, Rezai A. A Review of the Current Therapies, Challenges, and Future Directions of Transcranial Focused Ultrasound Technology: Advances in Diagnosis and Treatment. JAMA Neurol. 2018;75:246–254.
[168] Mainprize T, Lipsman N, Huang Y, et al. Blood-brain barrier opening in primary brain tumors with non-invasive MR-guided focused ultrasound: a clinical safety and feasibility study. Sci Rep. 2019;9:321.
[169] Huang Y, Alkins R, Schwartz ML, et al. Opening the Blood-Brain Barrier with MR Imaging–guided Focused Ultrasound: Preclinical Testing on a Trans–Human Skull Porcine Model. Radiology. 2017;282:123–130.
[170] Meng Y, Jones RM, Davidson B, et al. Technical Principles and Clinical Workflow of Transcranial MR-Guided Focused Ultrasound. Stereotact Funct Neurosurg. 2021;99:329–342.
[171] Meng Y, Pople CB, Suppiah S, et al. MR-guided focused ultrasound liquid biopsy enriches circulating biomarkers in patients with brain tumors. Neuro-Oncol. 2021;23:1789–1797.
[172] Chen K-T, Lin Y-J, Chai W-Y, et al. Neuronavigation-guided focused ultrasound (NaviFUS) for transcranial blood-brain barrier opening in recurrent glioblastoma patients: clinical trial protocol. Ann Transl Med. 2020;8:673.
[173] Chen K-T, Huang C-Y, Pai P-C, et al. Focused ultrasound combined with radiotherapy for malignant brain tumor: a preclinical and clinical study. J Neurooncol. 2023;165:535–545.
[174] Chen K-T, Chai W-Y, Lin Y-J, et al. Neuronavigation-guided focused ultrasound for transcranial blood-brain barrier opening and immunostimulation in brain tumors. Sci Adv. 2021;7:eabd0772.
[175] Asquier N, Bouchoux G, Canney M, et al. Blood-brain barrier disruption in humans using an implantable ultrasound device: quantification with MR images and correlation with local acoustic pressure. J Neurosurg. 2019;132:875–883.
[176] Carpentier A, Canney M, Vignot A, et al. Clinical trial of blood-brain barrier disruption by pulsed ultrasound. Sci Transl Med. 2016;8:343re2-343re2.
[177] Idbaih A, Canney M, Belin L, et al. Safety and Feasibility of Repeated and Transient Blood–Brain Barrier Disruption by Pulsed Ultrasound in Patients with Recurrent Glioblastoma. Clin Cancer Res. 2019;25:3793–3801.
[178] Sonabend AM, Stupp R. Overcoming the Blood–Brain Barrier with an Implantable Ultrasound Device. Clin Cancer Res. 2019;25:3750–3752.
[179] Sonabend AM, Gould A, Amidei C, et al. Repeated blood–brain barrier opening with an implantable ultrasound device for delivery of albumin-bound paclitaxel in patients with recurrent glioblastoma: a phase 1 trial. Lancet Oncol. 2023;24:509–522.

[180] Carpentier A, Stupp R, Sonabend AM, et al. Repeated blood–brain barrier opening with a nine-emitter implantable ultrasound device in combination with carboplatin in recurrent glioblastoma: a phase I/II clinical trial. Nat Commun. 2024;15:1650.
[181] ter Haar G, Shaw A, Pye S, et al. Guidance on reporting ultrasound exposure conditions for bio-effects studies. Ultrasound Med Biol. 2011;37:177–183.
[182] Padilla F, Ter Haar G. Recommendations for reporting therapeutic ultrasound treatment parameters. Ultrasound Med Biol. 2022;48:1299–1308.

Tables

Table 1 : Labels and possible entries screened for visualization.

LABEL	POSSIBLE ENTRIES
CITATION	Name YYYY
TYPE	Article / Review
DESCRIPTION	DOI
BIOEFFECT	Thermal ablation / Mechanical ablation / Drug delivery / Hyperthermia
PRESSURE RANGE	< 1 Mpa / 1-10 Mpa / > 10 Mpa
MONITORING/GUIDANCE MODALITY	Echography / MRI / Cavitation mapping / Cavitation detection / Elastography / QUS* / Simulation / Neuronavigation / Thermoprobe
TECHNOLOGY	Piezoceramic / Piezocomposite / MUT / DMUA / [Clinical device]**
STUDY SETTING	In vitro/ In silico / Ex vivo / In vivo / Clinical
TARGET/ORGAN	Liver / Kidney / Muscle / Brain / Vascular / Brain / Desmoid tumors / Limbs / Pancreas / Heart / Breast / Subcutaneous tumors
FREQUENCY	<1 MHz / 1-3 MHz / >3 MHz
F-NUMBER	<0.8 / 0.8-1.2 / >1.2
DUTY CYCLE	<2% / 2-99.9% / CW

*QUS includes Nakagami, strain imaging, US thermometry, entropy-based methods, backscatter characterization. ** Name of the clinical system

Table 2 : Summary of currently enrolling clinical trials, organized by targeted bioeffect. The trial title, targeted clinical indication, current enrollment status and number of patients anticipated to enroll on trial as well as clinical trial location are detailed.

Bioeffect	NCT/ Clinical Trial Name	Clinical Indication	Status/ Anticipated enrollment	Location
Mechanical ablation	NCT05820087/ HistoSonics: Treatment of Primary Solid Renal Tumors Using Histotripsy	Renal tumors	Recruiting/ 68	USA
	NCT05432232/ HistoSonics: Treatment of Primary Solid Renal Tumors Using Histotripsy	Renal tumors	Recruiting/ 20	UK
	NCT04572633/ HistoSonics: Treatment of Primary and Metastatic Liver Tumors Using Histotripsy	Primary and metastatic liver tumors	Active, not recruiting/ 47 (actual)	USA
	NCT04573881/ HistoSonics: Treatment of Primary and Metastatic Liver Tumors Using Histotripsy	Primary and metastatic liver tumors	Active, Not recruiting/ 24 (actual)	EU/UK
	NCT06282809/ HistoSonics: Treatment of Pancreatic Adenocarcinoma Using Histotripsy	Pancreatic Adenocarcinoma	Note yet recruiting/ 50	Spain
Drug Delivery	NCT03739905/ ExAblate BBB Opening for Treatment of Alzheimer's Disease	Alzheimer	Recruiting/ 30	Canada
	NCT05317858/ BBB Disruption Using ExAblate Focused Ultrasound With Standard of Care Treatment of NSCLC Brain Mets	Lung cancer metastases	Recruiting/ 20	USA, Canada, Korea
	NCT05565443/ MR-guided Focused Ultrasound Plus GCase	Parkinson	Recruiting/ 14	Canada
	NCT05864534/ Phase 2a Immune Modulation with Ultrasound for Newly Diagnosed Glioblastoma	GBM	Recruiting/ 25	USA

Bioeffect	NCT/ Clinical Trial Name	Clinical Indication	Status/ Anticipated enrollment	Location
	NCT05293197/ Safety Study of the Repeated Opening of the BBB With the SonoCloud® Device to Treat Malignant Brain Tumors in Pediatric Patients (SONOKID)	Pediatric malignant brain tumors	Recruiting/ 24	France
	NCT04528680/ Ultrasound-based BBB Opening and Albumin-bound Paclitaxel and Carboplatin for Recurrent Glioblastoma (SC9/ABX)	GBM	Recruiting/ 57	USA
	NCT05469009/ Safety and Feasibility of Exablate BBB Disruption for Mild Cognitive Impairment or Mild Alzheimer's Disease Undergoing Standard of Care Monoclonal Antibody (mAb) Therapy	Alzheimer	Recruiting/ 15	USA
	NCT05762419/ FUS Etoposide for DMG - A Feasibility Study	DMG	Active, Not recruiting/ 10	USA
	NCT05902169/ Sonocloud-9 in Association With Carboplatin Versus Standard-of-Care Chemotherapies (CCNU or TMZ) in Recurrent GBM (SONOBIRD)	GBM	Recruiting/ 560	USA, France, Belgium, Germany, Italy, Spain
Thermal ablation	NCT03948789/ Phase III Study of MR-Guided Focused Ultrasound Surgery for the Treatment of Uterine Fibroids Compared to Myomectomy	Uterine Fibroid	Recruiting/ 127	Germany
	NCT05569200/ The Clinical Trial about Treatment of Benign Uterus Myoma by Haifu Focused Ultrasound Tumor Therapeutic System	Uterine Fibroid	Not yet recruiting/ 10	Taipei
	NCT05386615/ Post ExAblate Pregnancy outcomes registry study: ExAblate treatment of symptomatic uterine fibroids	Uterine Fibroid	Recruiting/ 200	USA/China
	NCT02914704/ Treatment of Benign Uterine Disorders using High Intensity Focused Ultrasound (MR-HIFU)	Uterine Fibroid	Recruiting/ 500	Finland
	NCT05972642/ Safety & Efficacy of non-invasive procedures using ultrasound-guided HIFU 'Sonotrip V20' in symptomatic uterine fibroids	Uterine Fibroid	Not yet recruiting/ 30	Korea

Bioeffect	NCT/ Clinical Trial Name	Clinical Indication	Status/ Anticipated enrollment	Location
	NCT05044754/ SCAP vs HIFU for Recurrent Prostate Cancer After Radiation Therapy (SALVPROST)	Prostate cancer	Recruiting/ 50	France, Spain
	NCT06270043/ Focal Therapy for Localized Prostate Cancer	Prostate cancer	Recruiting/ 500	USA
	NCT04808427/ Pilot Study to Investigate Magnetic Resonance (MR) Image Guided Focal Therapy in Prostate Cancer	Prostate cancer	Recruiting/ 15	USA
	NCT04549688/ Active Surveillance Plus (AS+): High-intensity Focused Ultrasound (HIFU) in Patients With Localized Prostate Cancer	Prostate cancer	Recruiting/ 250	Norway
	NCT06178354/ Focal Ablation With Focal Cryotherapy or HIFU for the Treatment of Men With Localized Prostate Cancer	Prostate cancer	Recruiting/ 100	USA
	NCT06223295/ Effectiveness of Focal Therapy in Men With Prostate Cancer (ENFORCE)	Prostate cancer	Recruiting/ 356	Netherlands
	NCT05438563/ MRI-guided Transurethral Urethral Ultrasound Ablation for the Treatment of Intermediate Grade Prostate Cancer	Prostate cancer	Recruiting/ 15	USA
	NCT03620786/ HIFU for Focal Ablation of Prostate Tissue: An Observational Study	Prostate cancer	Recruiting/ 100	USA
	NCT01194648/ Focal Therapy for Prostate Cancer Using HIFU (INDEX)	Prostate cancer	Recruiting/ 354	UK
	NCT05001477/ Customized TULSA-PRO Ablation Registry (CARE)	Prostate cancer	Recruiting/ 1000	USA

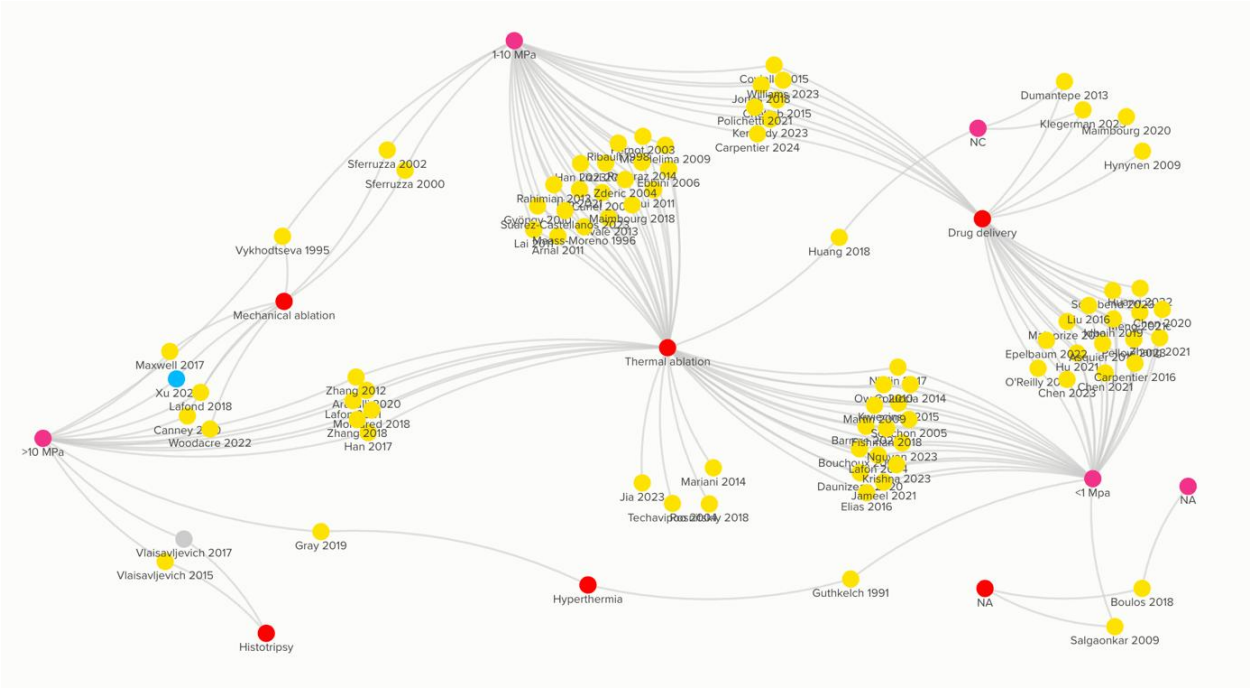
1-10 MPa
Sferruzza 2002
Sferruzza 2000
Vykhodtseva 1995
Mechanical ablation
Maxwell 2017
Xu 202
Lafond 2018
Canney 2
Woodacre 2022
>10 MPa
Zhang 2012
Zhang 2018
Han 2017
Gray 2019
Vlaisavljevich 2017
Vlaisavljevich 2015
Histotripsy
Hyperthermia
Thermal ablation
Mariani 2014
Jia 2023
Techavipoo
Guthkelch 1991
Huang 2018
Drug delivery
Dumantepe 2013
NC
Hynynen 2009
Liu 2016
Hu 2021
Carpentier 2016
Chen 2021
<1 Mpa
NA
Boulos 2018
Salgaonkar 2009

Figure 1

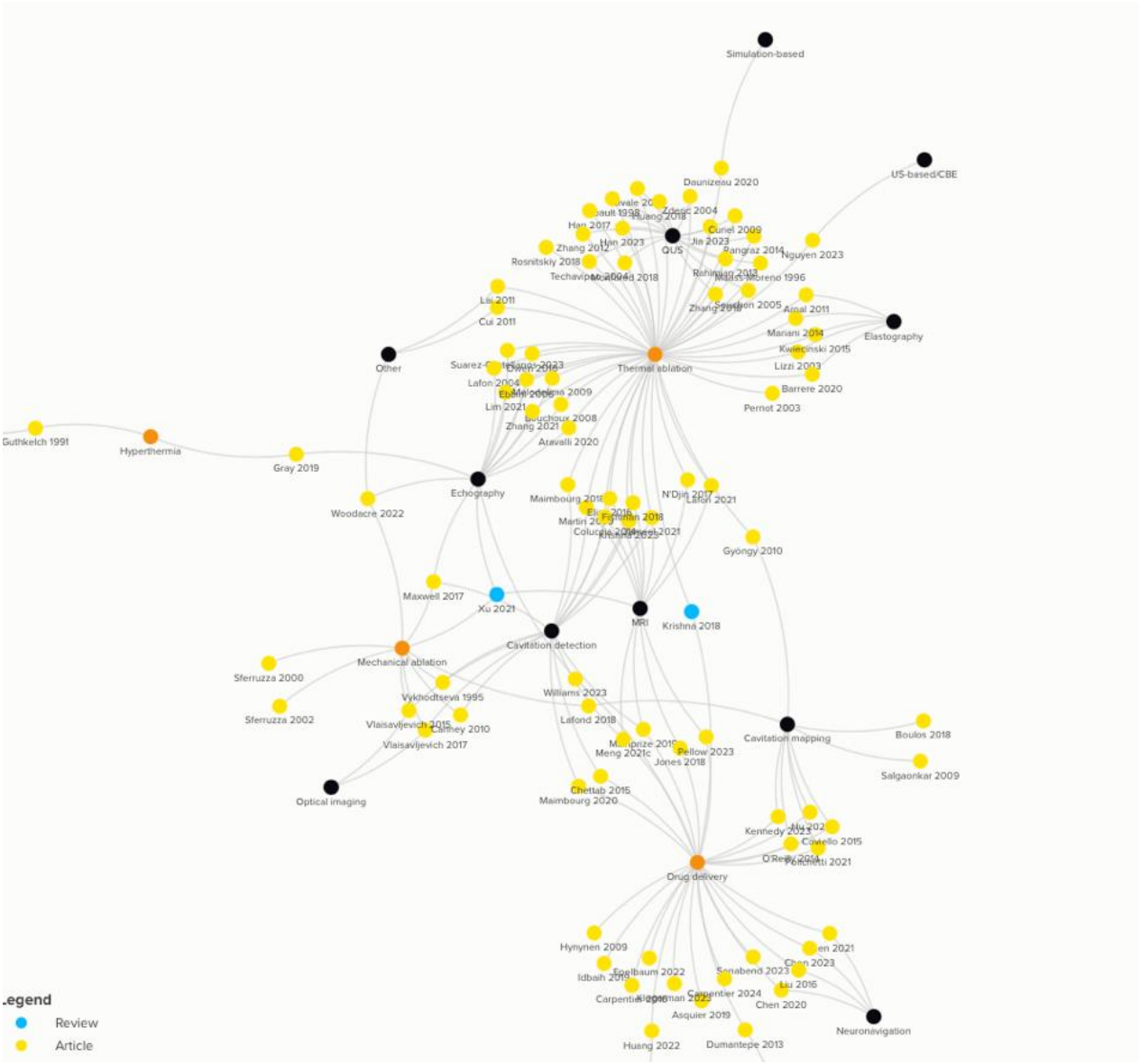
Simulation-based
US-based/CBE
Daunizeau 2020
Curiel 2009
Nguyen 2023
Rangraz 2014
QUS
Zhang 2012
Rosnitskiy 2018
Techavipoo 2004
Rahimian 2013
Mallas-Moreno 1996
Liu 2011
Cui 2011
Amal 2011
Mariani 2014
Elastography
Kwiecinski 2015
Other
Thermal ablation
Lizzi 2003
Barrere 2020
Pernot 2003
Lafon 2004
Lim 2021
Zhang 2021
Aravalli 2020
Guthkelch 1991
Hyperthermia
Gray 2019
Echography
Woodacre 2022
Maimbourg 2018
N'Djin 2017
Lafon 2021
Gyöngy 2010
Maxwell 2017
Xu 2021
MRI
Krishna 2018
Cavitation detection
Mechanical ablation
Sferruzza 2000
Sferruzza 2002
Vykhodtseva 1995
Vlaisavljevich 2015
Carney 2010
Vlaisavljevich 2017
Optical imaging
Williams 2023
Lafond 2018
Pellow 2023
Jones 2018
Chettab 2015
Maimbourg 2020
Cavitation mapping
Boulos 2018
Salgaonkar 2009
Kennedy 2023
Coviello 2015
Drug delivery
Hynynen 2009
Idbaih 2015
Eralbaum 2022
Sonabend 2023
Chen 2023
Liu 2016
Chen 2020
Asquier 2019
Huang 2022
Dumantepe 2013
Neuronavigation
Legend
Review
Article

Figure 2

Figure Captions

Figure 1: Visualization of the cited papers (yellow dots), clustering with bioeffects (red dots) and pressure range (pink dots).

Figure 2: Visualization of the cited papers (yellow dots), clustering with bioeffects (orange dots) and monitoring method (black dots).